Journal of
Applied Crystallography
ISSN 0021-8898

Received 14 July 2005
Accepted 7 October 2005

Design and performance of a thermal-neutron double-crystal diffractometer for USANS at NIST

J. G. Barker,[a]* C. J. Glinka,[a] J. J. Moyer,[a] M. H. Kim,[a] A. R. Drews[b] and M. Agamalian[c]

[a]NIST Center for Neutron Research, National Institute of Standards and Technology Gaithersburg, Maryland 20899, USA, [b]Ford Motor Company, Research and Advanced Engineering, Dearborn, Michigan 48121, USA, and [c]Oak Ridge National Laboratory, Oak Ridge, Tennessee 37831, USA. Correspondence e-mail: john.barker@nist.gov

An ultra-high-resolution small-angle neutron scattering (USANS) double-crystal diffractometer (DCD) is now in operation at the NIST Center for Neutron Research (NCNR). The instrument uses multiple reflections from large silicon (220) perfect single crystals, before and after the sample, to produce both high beam intensity and a low instrument background suitable for small-angle scattering measurements. The minimum detector background to beam intensity ratio (noise-to-signal, N/S) for $q \geq 5 \times 10^{-4}$ Å^{-1} is 4×10^{-7}. The instrument uses 2.38 Å wavelength neutrons on a dedicated thermal neutron beam port, producing a peak flux on the sample of 17300 cm^{-2} s^{-1}. The typical measurement range of the instrument extends from 3×10^{-5} Å^{-1} to 5×10^{-3} Å^{-1} in scattering wavevector (q), providing information on material structure over the size range from 0.1 μm to 20 μm. This paper describes the design and characteristics of the instrument, the mode of operation, and presents data that demonstrate the instrument's performance.

1. Introduction

The NCNR has constructed a high-intensity and low-background Bonse–Hart-type (Bonse & Hart, 1965) multiple-reflection DCD using perfect silicon crystals in order to extend the range of observable structures. The very high angular resolution provided by Bragg diffraction from perfect crystals extends the q range to much smaller momentum transfers than feasible from a pinhole-type instrument. Multiple reflections are needed to reduce the N/S ratio to below $\sim 10^{-3}$, needed for small-angle scattering measurements. Although the multiple-reflection DCD design has been routinely used for ultra-small-angle X-ray scattering (USAXS) measurements for many years, the technique has only recently had success in the neutron community due to previously unresolved background problems (Agamalian *et al.*, 1997) that are unique to USANS instruments. The NCNR instrument was designed with particular attention to both minimizing background and maximizing the beam intensity.

Neutron double-crystal diffractometers using single reflections before and after the sample have been in use since the 1960s (Shull *et al.*, 1967). Unfortunately, the background from the wings of the rocking curve often obscures the weaker small-angle scattering (SAS), except from the strongest scattering samples. The technique for reducing the reflectivity of the wings using multiple reflections from perfect single crystals before and after the sample was extended to neutron scattering instruments by Schwahn *et al.* (1985). Although this technique was partially successful, theoretical performance was not achieved and a strong parasitic instrument background component remained that was not seen in similar X-ray instruments. As a result, neutron measurements were successful only on rather strong scattering samples. The ability of neutrons to pass easily through several centimetres of silicon without appreciable absorption presented unique problems in the instrument design for neutron applications. By cutting the crystal and inserting an absorber between adjacent reflectors, Agamalian *et al.* (1997) were able to reduce the intensity of the parasitic background by two orders of magnitude and thus were the first to produce a rocking curve with N/S $\leq 10^{-4}$. Currently, several other DCD instruments of this type with low background (N/S $\leq 10^{-4}$) and high q resolution ($q_{\min} = 3 \times 10^{-5}$ Å^{-1}) are in operation around the world (Agamalian *et al.*, 1997; Bellmann *et al.*, 1998; Takahashi *et al.*, 1999; Borbely *et al.*, 2000; Hainbuchner *et al.*, 2000; Treimer *et al.*, 2001; Jericha *et al.*, 2003; Villa *et al.*, 2003) and there is a proposal to build a new time-of-flight DCD instrument at the Spallation Neutron Source that will utilize higher order reflections for even higher q resolution (Carpenter *et al.*, 2003).

2. Instrument concepts

Here we describe the basic operating principle of a double-crystal diffractometer. If a polychromatic (white) divergent beam is directed onto a perfect single crystal, a polychromatic

vertically and horizontally divergent diffracted beam is produced by Bragg reflection. (Throughout this article, the diffraction plane is assumed to be horizontal, with the vertical divergence limited by crystal size and spacing.) Although the horizontal divergence of the beam for any specific wavelength is very small (typically a few microradians), all neutrons with wavelengths and incidence angles that satisfy Bragg's Law will be diffracted, thus producing a polychromatic diffracted beam with a total horizontal divergence limited by the divergence of the source on the crystal. The first crystal in a DCD is commonly referred to as a 'monochromator', which we also adopt, despite the foregoing discussion. A perfect-crystal analyzer, with the same d spacing and oriented parallel to the monochromator, will diffract nearly all the beam accepted by the monochromator. Because the angle–wavelength correlation established by the monochromator is only satisfied at the analyzer when they are parallel, even a very small rotation of the analyzer will simultaneously destroy the Bragg condition for all neutrons falling on the analyzer.

If a sample is placed between the two crystals, and if the analyzer is rotated by a small angle (θ) from the aligned condition, all neutrons undergoing small-angle scattering through a horizontal angle θ in the same direction as the analyzer rotation are reflected into the detector, while unscattered neutrons will be transmitted. Scattering in the vertical direction does not affect fulfillment of the Bragg condition. By placing a detector to collect only the diffracted beam from the analyzer, the diffractometer measures the scattered intensity from the sample with excellent horizontal angular resolution, but with very poor vertical resolution. An analogous slit smearing condition arises when long narrow slits are used to provide angular collimation in one direction only.

A double-crystal diffractometer yields superior scattered intensity compared with pinhole instruments under ultra-high-resolution conditions (Schelten & Hendricks, 1978) with the detector count rate $C_{\rm D}(q)$ at a given value of momentum transfer $q \simeq 2\pi\theta/\lambda$ varying with the minimum resolvable q value, $q_{\rm min}$, as $C_{\rm D} \simeq q_{\rm min}^2$, whereas pinhole collimation produces $C_{\rm D}(q) \simeq q_{\rm min}^4$. The DCD has the further advantage in that its q resolution is independent of beam size, a feature that is particularly suited to neutron instruments. The DCD has the disadvantages that the measured scattering is strongly smeared, and that only one q value can be measured at a time, whereas pinhole collimated instruments utilize two-dimensional detectors to collect data at 25 to 50 q values of equivalent solid angle at the same time.

3. Rocking curve

The reflectivity curve $R_{\rm D}$ produced by Bragg diffraction from the front face of a thick perfect crystal follows the relation (Zachariasen, 1967; Wagh *et al.*, 2001; Villa *et al.*, 2003)

$$R_{\rm D}(y) = \begin{cases} 1 & |y| \le 1, \\ [|y| - (y^2-1)^{1/2}]^2 & |y| > 1, \end{cases} \qquad (1)$$

Table 1
Specific angular width Δ^* such that $R_{nm}(\Delta^*) = 1 \times 10^{-3}$ for DCD having m reflections in the monochromator and n reflections in the analyzer.

The Ewald formula is appropriate for neutron-transparent crystals where both front- and back-face reflections occur. The Darwin formula is appropriate for highly absorbing crystals used in X-ray scattering and special-shaped crystals for neutrons (Wagh *et al.*, 2001; Villa *et al.*, 2003).

$m \times n$	Ewald	Darwin
1×1	37	25
2×2	5.13	3.75
3×3	3.04	2.46
4×4	2.51	2.19
5×5	2.30	2.09

where $y = \theta/\Delta\theta_{\rm D}$ is the reduced angle, θ is the difference in angle of incidence and the Bragg diffraction angle $\theta_{\rm B}$ for the diffracting plane, and $\Delta\theta_{\rm D}$ is the Darwin half-width.

For thermal neutrons, most crystals are weakly absorbing and the back face reflection also contributes to the total reflectivity according to the Ewald formula (Takahashi & Hashimoto, 1995):

$$R_{\rm E}(y) = 2R_{\rm D}(y)/[1 + R_{\rm D}(y)]. \qquad (2)$$

The rocking curve obtained by rotating the analyzer, with m monochromator reflections and n analyzer reflections, is the convolution of the appropriate reflectivity formula (R),

$$R_{nm}(\Delta) = \int_{-\infty}^{\infty} R(y)^n R(y-\Delta)^m \, {\rm d}y. \qquad (3)$$

Typically, the small-angle scattering intensity is $<1 \times 10^{-3}$ of the beam intensity. Thus, the usable q range is limited to that region where the wings of the rocking curve $R_{nm}(\Delta) \le 1 \times 10^{-3}$. Table 1 lists the specific reduced angle Δ^*, where $R_{nm}(\Delta^*) = 1 \times 10^{-3}$, depending upon the number of reflections. To have sufficient reduction of the wings, at least 2×2 reflections are needed. To maximize space utilization, and to optimize shielding design, a neutron DCD will typically use an odd number of reflections, either in a 3×3 or 5×5 reflection geometry.

For symmetrically cut crystals (crystal plane is parallel to the surface), the half-width of the Bragg reflection $\Delta\theta_{\rm D}$ is given by

$$\Delta\theta_{\rm D} = \exp(-W) b_{\rm c} |F_{hkl}| N\lambda^2/[\pi \sin(2\theta_{\rm B})], \qquad (4)$$

where W is the Debye–Waller factor, $b_{\rm c}$ is the coherent scattering length per atom, F_{hkl} is the scattering amplitude for the (hkl) Bragg reflection, N is the number of unit cells per unit volume, and λ is the neutron wavelength. Although a large number of different high-quality single-crystal materials exist (Alexandropoulos & Cohen, 1974), the extremely high crystalline perfection and the large crystal size needed in this application have restricted use to either silicon or germanium. For silicon (220), $b_{\rm c} = 4.149 \times 10^{-15}$ m (Sears, 1984), $|F_{hkl}| = 8$, $N = 6.24 \times 10^{21}$ cm^{-3}, and at neutron wavelength $\lambda = 2.38$ Å, $\theta_{\rm B} = 0.670$ rad (38.4°), and $W = 0.03$ (Graf *et al.*, 1981), yielding $\Delta\theta_{\rm D} = 3.72 \times 10^{-6}$ rad. The current instrument has $n = m = 3$ reflections, which from Table 1 yields $\Delta^* = 3.04$. The

predicted minimum q that produces N/S = 1×10^{-3} is $q_{min} = (2\pi/\lambda)\Delta^*\Delta\theta_D = 3.0 \times 10^{-5}$ Å^{-1}.

Due to the smaller scattering length, the Darwin width $\Delta\theta_D$ produced by scattering of neutrons is a factor of 0.105 times the width produced from X-ray scattering from silicon crystals, if the same crystal reflection and wavelength are used. Thus, neutrons can probe structural features typically ten times larger than that observable from X-rays using DCDs. [Alternatively, a high-index (small d spacing) reflection, such as Si(1391), in combination with shorter wavelength can yield q resolution q_{min} using X-rays equivalent to the current neutron DCDs. Such a higher resolution high-index X-ray instrument has yet to be built.]

X-ray DCDs at synchrotrons can have up to eight orders of magnitude greater beam intensity than the current neutron DCD. Thus, for studies where there is acceptable contrast and available q range from X-rays and where suitably thin samples can be prepared, X-ray scattering is the preferred radiation. Likewise, static light scattering offers higher flux over the same q range as a neutron DCD for specimens that are optically transparent and with sufficient contrast. There are, however, many systems where these criteria are not satisfied and neutron scattering is preferred, such as for turbid or opaque specimens and for systems where there is too little optical or X-ray contrast for the features of interest.

4. Instrument design

To maximize the beam intensity, both the vertical and horizontal divergence collected from the neutron source is maximized. This requires a compact instrument with large crystals either placed close to the source or with the implementation of focusing optics. In addition, a wavelength close to the maximum of the Maxwellian distribution of the neutron spectrum is favored. The design must also consider minimizing the background from both thermal and fast neutron sources. This section briefly highlights some of the important instrument design features.

Fig. 1 shows schematically the layout of the instrument. Because of limited space between adjacent instruments, and to allow room at the sample position for ancillary equipment, the monochromator (M) had to be located at least 2 m from the reactor face. To increase source divergence collected, a doubly curved graphite premonochromator (PM) was introduced before the monochromator to focus the beam at sample position (S). The vertical focusing increases the current density at the sample by a factor of three as estimated from acceptance diagrams (Copley, 1991). Twenty, 0.2 cm thick, graphite (002)-oriented crystals are attached with aluminium clips in five rows by four columns to a faceted aluminium frame, forming a reflector surface 10 cm high and 18 cm long. Each facet of the frame is tangent to a toroid having a vertical radius of curvature of 60 cm, and a horizontal radius of curvature of 1000 cm.

Increasing the horizontal source divergence increases the beam intensity by broadening the range of wavelengths accepted by the monochromator. Freund (1983) has demonstrated that the effective horizontal source divergence incident upon a monochromator can be increased by twice the mosaic spread of the PM if the relation $d_{PM}^2 = 4d_M^2 - 3\lambda^2/4$ is maintained. The combination of mosaic graphite (002) crystals for the PM (d spacing d_{PM} = 3.354 Å) and an Si(220) crystal for the M (d_M = 1.92 Å), has an optimum wavelength λ_{opt} = 2.16 Å. Despite the fact that we are using the less than optimal wavelength λ = 2.38 Å, only 4% of the divergence viewed at monochromator is from the reactor source, and 96% is supplied by the mosaic spread of graphite. The 0.012 rad FWHM (full width at half-maximum) mosaic spread of the PM increases the effective horizontal source divergence to 0.024 rad (1.3°). By curving the PM horizontally, the horizontal divergence is increased by a further factor of two.

A disadvantage of Si(220) crystals for the M/A is contamination by scattering of higher order ($\lambda/2$) wavelengths which are reflected by the crystals at the same Bragg angle. By shifting the instrument wavelength slightly to λ = 2.38 Å, an oriented graphite beam filter will efficiently attenuate the $\lambda/2$ component in the white beam by scattering from the 118, 114, 116 and 101 reflections without large losses in the λ component (Shapiro & Chesser, 1972; Frikkee, 1975). Our graphite filter (GF) is 2.7 cm thick and is placed in a duct immediately after the shutter, with its c axis aligned along the beam direction. The FWHM mosaic spread of the graphite filter was measured to be 0.047 rad (2.7°). From a refraction measurement, we estimate the transmission of the $\lambda/2$ component to be 0.002, which is sufficiently small that its contribution to the SAS data can be neglected. The transmission of the λ component was measured to be 0.91. It should be noted that

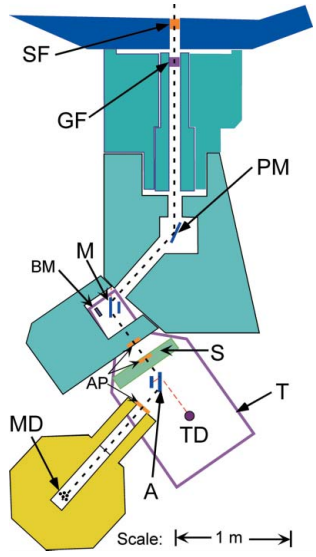

Figure 1
A schematic layout of the perfect crystal diffractometer. The dashed line indicates the beam path. The main instrument components as described in the text are: sapphire filter (SF), pyrolytic graphite filter (GF), graphite premonochromator (PM), silicon monochromator (M), beam monitor (BM), sample changer (S), silicon analyzer (A), transmission detector (TD), vibration isolation table (T), beam apertures (AP), and the main detector (MD). Both MD and A are mounted on precision slides, allowing placement of large ancillary equipment on a hidden sample table.

misorientation of the graphite filter by more than 0.09 rad (5°) from the beam direction can severely attenuate the λ component *via* the 103 reflection.

Both the monochromator (M) and the analyzer (A) are channel-cut triple-bounce silicon (220) crystals. Since resolution is independent of sample size in this type of instrument, large crystals are used to provide a beam cross section at the sample of up to 5 cm by 5 cm. A machined gap of 3 cm separates the first and third reflectors as shown in Fig. 2. The crystals are relief etched after machining, revealing an orange peel surface and straight lines from the machining process. Both crystals are mounted on a three-leg pneumatic isolation table (T) for vibration damping. Mounted directly behind M (see Fig. 1) is a low-efficiency beam monitor (BM) of the fission chamber type for monitoring changes in beam current density.

There are two sample positions supported independently from the isolation table (see Fig. 3). For routine use, a translation slide is used to move multi-position sample holders. The slide is cantilevered by distance of 50 cm from a permanently mounted sample table located within the isolation table. To accommodate large ancillary equipment, the sample area can be enlarged by 50 cm by translating both the analyzer and the detector out on precision slides, revealing a large 58 cm diameter secondary sample table mounted inside of the isolation table. The secondary position has the beam intensity reduced by factor of 0.6 from the effect of defocusing. The fixed table can support large furnaces, cryostats, or magnets up to 300 kg.

A thermal neutron shielded box (not shown in Fig. 3) covers the analyzer slide, thus shielding both transmission and main detectors from the ambient thermal neutron background [0.5 (2) cm^{-2} s^{-1}]. Entrance and exit cutouts to the box allow the analyzer-reflected beam to travel to the main detector. The analyzer stage is driven by a micrometer screw attached to a tangent arm with a 0.010 μrad (2×10^{-3} arcsec) resolution. The vertical tilts of the M and A crystals are controlled with separate tilt stages with an accuracy of 0.3 μrad (0.06 arcsec).

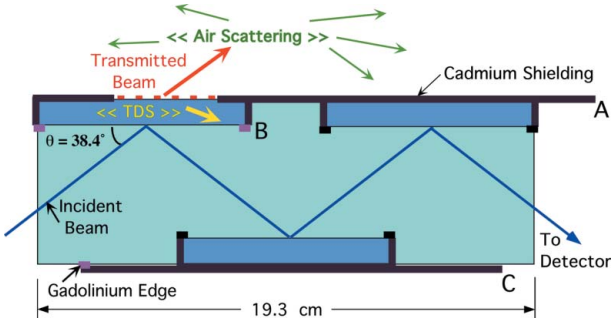

Figure 2
Top view of the analyzer. Thick lines represent the cadmium shielding. Arrows represent the path of the 5 cm wide beam. The edges of the cadmium shielding in contact with the beam before the first reflection are lined with gadolinium foil to minimize background from beam refraction. A 20 mm radius aperture is cut into the shield behind the first reflector to allow the transmitted main beam to travel to the transmission detector. The shielding at the back of the third reflector (A) blocks the air scattering from the transmitted beam from reaching the detector. Thermal diffuse scattering from the first reflection is blocked by shielding located at B and C. Dynamic propagation of neutrons *via* Garland reflections is blocked from reaching the third reflector by shielding located at point B.

5. Background reduction

Small strains within the crystal are known to increase the background significantly in the wings of the reflectivity (Agamalian *et al.*, 2001). We have found that even lightly tightening small nylon set screws against the 16 mm thick base of a crystal to prevent lateral motion is sufficient to produce a large increase in the parasitic background. To minimize strains, the crystals currently rest freely within the holders without any clamping.

Strains in the crystals can also arise from imperfections such as precipitates (Borghesi *et al.*, 1995) or from distortion due to gravity. To reduce the likelihood of these strain sources, our crystals were machined from zero-dislocation-type boules of float-zone refined silicon. Crystals grown by the float-zone method is preferred over Czochralski pulling method (CZ) due to both the higher overall crystalline perfection and the lower oxygen levels. The relatively thick reflectors (10 mm) and base (16 mm) of the channel-cut crystals also increases their rigidity, and minimizes strains produced by gravity.

To achieve a low instrument background, we have identified five additional sources of neutron background that must be shielded from the detector: (i) fast neutrons, (ii) air scattering, (iii) thermal diffuse scattering, (iv) single reflection paths produced by dynamical diffraction, and (v) scattering from the edges of apertures.

The background from fast neutrons penetrating the detector shielding must in particular be minimized. The small fast neutron cross sections of all materials require shield thicknesses typically measured in tens of centimetres. Composite shields containing both hydrogen and iron are most effective at reducing neutron energies down to the

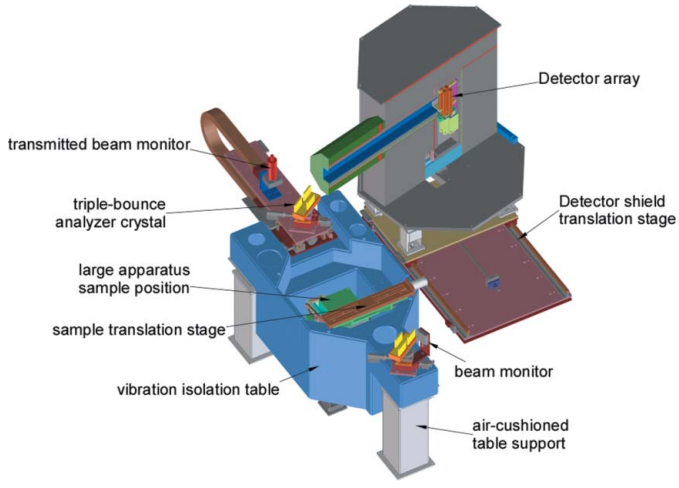

Figure 3
Three-dimensional view of the accessible part of the instrument illustrating the two sample locations. The shields covering both crystals were removed for clarity. The detector shield is also cut to allow viewing of the internal duct and detectors.

thermal range where they can be absorbed. Shields containing 50 vol.% steel shot in wax surround the beam path before the sample position and a 0.5 m thick shield made from high-density polyethylene surrounds the detector. As shown in Fig. 1, the detector is close to the line of sight of the beam exiting the reactor core. Only a 0.6 m thick shield located immediately after PM and the 0.5 m thick detector shield protect the detector from fast neutrons that exit the beam tube.

To reduce the fast neutron flux in the direction of the detector, an 11 cm long single-crystal Al_2O_3 sapphire filter (SF) was located inside the reactor shutter beam tube 4 m from the detector. Sapphire crystals can be used to scatter fast neutrons into the surrounding shielding preferentially, thereby significantly lowering the fast neutron background at the detector. The total scattering cross section for sapphire varies from 0.35 (2) cm^{-1} to 0.16 (1) cm^{-1} over the neutron energy range of 1 MeV to 10 MeV (Stehn *et al.*, 1964), while the total scattering cross section at the instrument wavelength λ = 2.38 Å (14.2 meV) is 0.026 (1) cm^{-1} (Mildner & Lamaze, 1998), resulting in a transmission of 0.75. Thus, the sapphire filter preferentially transmits thermal (λ = 2.38 Å) neutrons *versus* fast neutrons by a ratio varying from 35 to 4.4 over the 1 MeV to 10 MeV energy range. For sapphire crystals with their *c* axis aligned along the beam direction, Bragg scattering for λ = 2.363 Å from the 10$\bar{1}$0 reflection and at λ = 2.369 Å from 116 reflection will reduce the transmitted beam within the accepted wavelength spread. Thus, high-quality crystals with small mosaic spread are needed to minimize these losses from Bragg scattering.

Background from air scattering of the main beam that occurs after transmission through the first analyzer reflector can reach the detector by transmission through the third analyzer reflector. In addition, thermal diffuse scattering (TDS) from phonons in the analyzer's first reflector can redirect neutrons into the detector. By inserting a second germanium analyzer crystal, Mook (1974) observed a factor of 20 reduction in the background, which was attributed to removing the first analyzer crystal from the detector's view, thus eliminating TDS background originating from the intense main beam. Fig. 2 shows that both the TDS and air scattering background components can be shielded from the detector by appropriate placement of cadmium shielding around the crystal. In particular, shielding on the back of the third analyzer reflector is effective in blocking air scattering. Inserting shielding in the gap between the first and third reflectors, and on the back of the second reflector is effective in removing the TDS background.

As originally identified by Agamalian *et al.* (1997), the dynamical propagation of neutrons throughout the crystal can allow single reflection paths to the detector producing a high background ($I_B \simeq q^{-2}$). For a three-bounce channel-cut crystal with thick reflectors and the first and third reflectors adjacent to one another, neutrons reflecting off the back face of the first reflector near the third reflector can bypass the second reflector entirely. Alternatively, neutrons will propagate down the length of the first reflector by multiple Garland reflections inside the crystal if the crystals are bent slightly (Agamalian *et al.*, 2001) and can emerge near the third reflector in the direction of the detector. A gap machined between the first and third reflectors and filled with a cadmium absorber eliminates both of these single reflection pathways to the detector.

Refraction from edges of apertures placed between the last monochromator reflection and the first analyzer reflection can also produce parasitic background (Treimer *et al.*, 2002). This can largely be avoided if the edges of the cadmium apertures between the last monochromator reflection and the first analyzer reflection are covered with 0.13 mm thick gadolinium foil. Gadolinium has a factor 13 lower penetration depth than cadmium (depth for 1/*e* transmission = 5 µm *versus* 65 µm at λ = 2.38 Å) due to its higher absorption cross section.

6. Performance

The wavelength distribution was calculated from the angular distribution measured by locating a fixed narrow slit at the sample, and scanning a second narrow slit at the detector. The wavelength distribution was nearly rectangular in shape with an FWHM $\Delta\lambda$ = 0.141 (5) Å, corresponding to a spread $\Delta\lambda/\lambda$ = 5.9 (2)%. This spread is significantly larger than other neutron DCD-type instruments, but is smaller than that typically used in pinhole-type SANS instruments (Glinka *et al.*, 1998). Smearing produced by the wavelength distribution significantly affects the instrument resolution only when diffraction spots, such as from superconducting fluxoid lattices or line gratings, are being investigated.

The maximum beam intensity is 57400 s^{-1}. Scanning a narrow slit at the sample position both vertically and horizontally revealed an approximate Gaussian-shaped beam profile with FWHM values of 25 mm horizontally and 28 mm vertically. Using circular apertures with radii from 3 mm to 22 mm to define the beam, a simple polynomial expression for the beam intensity dependence on aperture radius was determined by fitting to $I_B = 662R^2 - 39.9R^3 + 0.70R^4$ (with I_B having units of s^{-1} and R having units of mm). The peak current density at the center of the beam was 17300 cm^{-2} s^{-1}, measured using the smallest (3 mm) radius aperture, and is a factor of two higher than the next highest available on the S18 instrument at the ILL (Hainbuchner *et al.*, 2000).

We can compare the measured peak current density to an estimate of the expected peak current density at the sample position from measured geometric and component factors using the expression

$$\varphi_B = \frac{d\varphi_S}{d\lambda\, d\Omega}(\lambda)\Delta\lambda\Delta\Omega_S T_L G \qquad (5)$$

where φ_S is the integrated flux of the reactor source, $\Delta\lambda$ is the range of wavelength transmitted by monochromating system, $\Delta\Omega_S$ is the solid angle collected by the collimation system, T_L is the effective transmission (produced by attenuation of filters, air, *etc.*) and G is the gain from focusing. The reactor spectrum closely follows a Maxwellian shape with differential flux,

$$\frac{d\varphi_S}{d\lambda\, d\Omega}(\lambda) = \frac{\varphi_0}{2\pi}\frac{\lambda_T^4}{\lambda^5}\exp\left(\frac{-\lambda_T^2}{\lambda^2}\right), \quad (6)$$

where φ_0 is the integrated flux of the source with a wavelength distribution, $\lambda_T = AT^{-1/2}$, with $A = 30.9$ Å $K^{1/2}$, and T the temperature of the moderator. The thermal beam tube BT-5 at the NIST reactor produces a flux $\varphi_0 = 9.0 \times 10^{13}$ cm^{-2} s^{-1} and $\lambda_T = 1.70$ Å with an effective moderator temperature of 330 K (Cook, 2004). At a neutron wavelength $\lambda = 2.38$ Å, the differential flux of the source is estimated to be $d\varphi_S/d\lambda/d\Omega(\lambda) = 9.4 \times 10^{11}$ cm^{-2} s^{-1} sr^{-1} Å^{-1}. The distance from the shutter to the sample is 309 cm and the opening in the beam shutter is 6.7 cm × 6.7 cm. The vertical divergence of the source is then $\Delta\theta_Z = 6.7$ cm/309 cm = 0.022 rad. The horizontal divergence is approximately equal to twice the Darwin half-width, $\Delta\theta_Y = 2\Delta\theta_D = 7.4 \times 10^{-6}$ rad, and the solid angle of the source is then $\Delta\Omega_S \simeq \Delta\theta_D\Delta\theta_Z = 1.6 \times 10^{-7}$ sr.

Intensity is lost from attenuation from several different instrument components. The estimated transmission from 11 cm of sapphire is 0.75, from 1.6 cm of graphite is 0.91, and from 675 cm of air is 0.71. Assuming ideally imperfect crystals (Bacon & Lowde, 1948), the average reflectivity of the PM (Cook, 2004) is estimated as 0.76. The detector efficiency is 0.84. The effective transmission from all factors is estimated to be 0.31. Acceptance-diagram calculations (Copley, 1991) indicate that vertical focusing should increase the intensity by a factor $G = 3.1$. From equation (5), we estimate the beam current density at the sample to be 20500 cm^{-2} s^{-1}, which is 18% higher than the measured value of 17300 cm^{-2} s^{-1}.

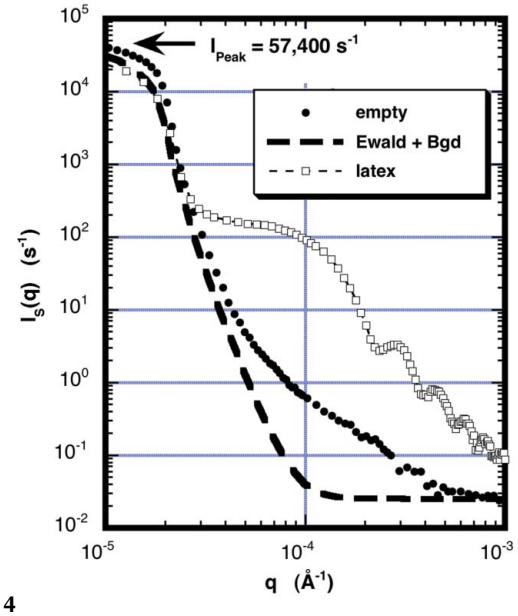

Figure 4
Plot of the measured and theoretical rocking curve. The solid circle symbols were measured with a 22 mm radius cadmium aperture. The dashed line is the theoretical curve obtained for 3 × 3 Ewald reflections [equations (1)–(3)] plus a flat background of 0.025 s^{-1}. The empty square symbols are the scattering from a 0.8% volume fraction of nearly monodisperse 4 µm diameter polystyrene spheres in 47% D_2O/53% H_2O solution. The sample scattered an estimated 5% of the total beam intensity. The maximum scattered intensity measured in the Guinier region was 200 s^{-1}, which is a 0.003 fraction of the beam intensity.

Fig. 4 shows the experimental rocking curve obtained using a 22 mm radius cadmium sample aperture (solid circles). Also shown is a theoretical curve (dashes) produced by multiplying the beam intensity (57400 s^{-1}) by the rocking curve [equations (1)–(3)] with the addition of a constant background component (0.025 s^{-1}). The difference between the experimental and theoretical curves is termed the 'parasitic' component to the instrument background. The FWHM of the curve is equal to $\Gamma_{1/2} = 2.0 \times 10^{-5}$ Å^{-1}. At $q = 2T_{1/2} = 4.0 \times 10^{-5}$ Å^{-1}, N/S = 2×10^{-4}, which is a factor two lower than that reported by Borbely *et al.* (2000). At $q \geq 5 \times 10^{-4}$ Å^{-1}, N/S = 4×10^{-7}, which is one to two orders of magnitude to lower than other instruments. This lower background allows measurements to be extended to higher q than on other instruments.

Measurements have determined that the remaining flat background of 0.025 s^{-1} is composed of 55% fast neutrons, 35% thermal neutrons, and 10% electronic noise. Note that by removing the piece of cadmium shielding on the back of the first and third analyzer reflectors (denoted as A in Fig. 2), the flat background increases by an order magnitude to 0.28 s^{-1}, predominantly from air scattering.

The remaining parasitic background, although much improved from earlier neutron instruments of this type, still limits the capability of the instrument to resolve weak scattering, particularly for $q \leq 2 \times 10^{-4}$ Å^{-1}. When smaller Cd apertures are used, we have noticed that the parasitic component depends to some extent upon refraction from the aperture edge, as studied by Treimer *et al.* (2002). The background is produced by the prismatic refraction of the divergent beam incident upon a straight cut aperture edge. This effect can be mitigated if the apertures are made from a more highly absorbing material, such as Gd, which reduces the depth of penetration into the edge. To test the improvement of

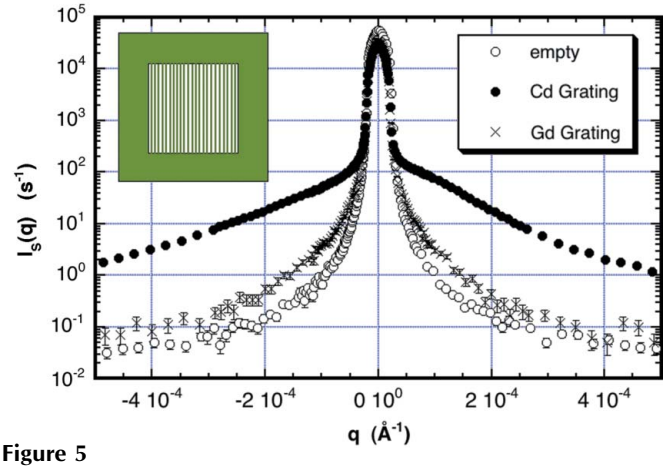

Figure 5
The graph shows the measured background from a 38 mm × 38 mm beam that is empty (open circles), or is covered with vertical gratings made from either 1 mm thick Cd (filled circles) or 0.13 mm thick Gd (crosses). Both gratings have 24 lines that are 0.8 mm wide. The large length of exposed edge of the grating produces a sizable background from Cd, but not from Gd. The reduction in background produced by replacing Cd with Gd is attributed to the reduced penetration depth limiting the fraction of the beam refracted by the aperture edge.

Table 2
Characteristics of the BT-5 DCD instrument.

Premonochromator	Pyrolytic graphite PG(002)
Mean wavelength	2.38 Å (range 2.31–2.45 Å)
Monochromator	Si(220)
Sample size	3–22 mm radius
Beam intensity	57400 s^{-1} (22 mm beam radius)
Peak beam current density	17300 cm^{-2} s^{-1}
Noise-to-signal (N/S)	
at $q = 2\Gamma_{1/2} = 4 \times 10^{-5}$ $Å^{-1}$	2×10^{-4}
at $q \geq 25\Gamma_{1/2} = 5 \times 10^{-4}$ $Å^{-1}$	4×10^{-7}
q range	3×10^{-5} $Å^{-1}$ to 0.005 $Å^{-1}$
q resolution ($\Gamma_{1/2}$)	2.0×10^{-5} $Å^{-1}$ (horizontal)
Size regime	0.1–20 μm

replacing Cd with Gd in the beam-defining sample apertures, two 24 line, 0.8 mm wide grates were made from a 1 mm thick Cd sheet and a 0.13 mm thick Gd foil. Fig. 5 shows the measured rocking curves with and without the grates (oriented in the vertical direction). The Cd grating increases the parasitic background by nearly two orders of magnitude over that measured without a grate, whereas the Gd grate increases the parasitic background a more modest factor of three. To limit the impact of this contribution to the background for smaller samples, we have fabricated 8 mm radius sample apertures from Gd foil for use with smaller samples.

Further improvement in parasitic background may be achieved by having cleaner, smoother and tapered aperture edges. The angular deflection of the beam from refraction can be limited to $q \leq 5 \times 10^{-6}$ $Å^{-1}$ if the edge angle is changed from the current straight cut of $\pi/2$ rad (90°) to a tapered cut of $\pi/4$ rad (45°), although the edge must come uniformly to a point on a sub-micrometre length scale.

Additional contributions to the parasitic background may arise from strains or surface roughness in the crystals. Although the relief-etch after machining was intended to eliminate strains at the crystal surfaces, it may be that small-angle scattering from the 'orange peel' surface of the last monochromator reflector contributes to the background. Likewise, internal defects within the crystal may also contribute to the remaining background.

Table 2 summarizes the performance characteristics of this instrument. Particular improvements of the current instrument over other instruments of this type are the highest reported beam current density (17300 cm^{-2} s^{-1}) and for $q \geq 5 \times 10^{-4}$ $Å^{-1}$ the lowest noise-to-signal ratio (4×10^{-7}). To demonstrate the capabilities of the instrument, we have measured scattering from a 0.8 vol.% suspension of 4 μm diameter spherical latex particles (empty square symbols in Fig. 4) in 47% D_2O/53% H_2O with a 2 mm thick cell. For this sample, the determination of the scattering profile shape extends over a range of 5000 between the maximum intensity measured in the forward direction (Guinier region) and the flat instrument background. The ratio of the maximum scattered intensity to the beam intensity is 0.003, with the sample scattering ∼5% of the beam at small angles (to avoid significant multiple scattering corrections, the sample should not scatter more than 10% of the beam). Thus, the present example covers nearly the largest range in scattered intensity observable with the current instrument without significant multiple scattering, and highlights its full potential.

7. Summary

Recent developments in understanding the sources of background in ultra-small-angle neutron scattering (USANS) instruments have led to the development of several new instruments. By applying the lessons learned from other instruments and optimizing our design for maximum intensity and minimum background, we have achieved higher beam intensity and lower noise-to-signal ratio for $q \geq 5 \times 10^{-4}$ $Å^{-1}$ than available on any other USANS instrument. The high resolution of the current instrument allows the investigation of structural sizes ranging from 0.1 μm to 20 μm. By focusing the beam at the sample with a doubly curved graphite mosaic premonochromator, the current density is increased by an estimated factor of six, taking advantage of the large wavelength spread that this DCD can accept ($\Delta\lambda/\lambda$ = 5.9%) (Freund, 1983). We have also identified six separate sources of background and described techniques for their mitigation.

Partial funding of the construction and operation of the DCD instrument is provided by the National Science Foundation under agreement No. DMR-9986442. Paul Brand, Andy Clarkson, Mike Rinehart, George Baltic, Scot Slifer, Doris Kulp, Thuan Thai and Nick Maliszewskyj provided technical help during the design and construction of the instrument, and Jeremy Cook provided Monte Carlo calculations of the reactor source spectrum and estimation of the graphite reflectivity. David Mildner provided an insightful editorial review.

References

Agamalian, M., Iolin, E., Kaiser, H., Rehm, C. & Werner, S. A. (2001). *Phys. Rev. B*, **64**, 161402.
Agamalian, M., Wignall, G. D. & Triolo, R. (1997). *J. Appl. Cryst.* **30**, 345–352.
Alexandropoulos, N. G. & Cohen, G. G. (1974). *Applied Spectroscopy*, **28**, 155–164.
Bacon, G. E. & Lowde, R. D. (1948). *Acta Cryst.* **1**, 303–314.
Bellmann, D., Klatt, M., Kampmann, R. & Wagner, R. (1998). *Physica B*, **241–243**, 71–73.
Bonse, U. & Hart, M. (1965). *Appl. Phys. Lett.* **7**, 238–240.
Borbely, S., Heiderich, M., Schwahn, D. & Seidl, E. (2000). *Physica B*, **276–278**, 138–139.
Borghesi, A., Pivac, B., Sassella, A. & Stella, A. (1995). *J. Appl. Phys.* **77**, 4169–4244.
Carpenter, J. M., Agamalian, M., Littrell, K. C., Thiyagarajan, P. & Rehm, C. (2003). *J. Appl. Cryst.* **36**, 763–768.
Cook, J. C. (2004). Private communication.
Copley, J. R. D. (1991). *Nucl. Instrum. Methods A*, **301**, 191–201.
Freund, A. K. (1983). *Nucl. Instrum. Methods*, **216**, 269–274.
Frikkee, E. (1975). *Nucl. Instrum. Methods*, **125**, 307–312.
Glinka, C. J., Barker, J. G., Hammouda, B., Krueger, S., Moyer, J. & Orts, W. J. (1998). *J. Appl. Cryst.* **31**, 430–445.
Graf, H. A., Schneider, J. R., Freund, A. K. & Lehmann, M. S. (1981). *Acta Cryst.* A**37**, 863–871.

Hainbuchner, M., Villa, M., Kroupa, G., Bruckner, G., Baron, M., Amenitsch, H., Seidl, E. & Rauch, H. (2000). *J. Appl. Cryst.* **33**, 851–854.
Jericha, E., Baron, M., Hainbuchner, M., Loidl, R., Villa, M. & Rauch, H. (2003). *J. Appl. Cryst.* **36**, 778–782.
Mildner, D. F. R. & Lamaze, G. P. (1998). *J. Appl. Cryst.* **31**, 835–840.
Mook, H. A. (1974). *J. Appl. Phys.* **45**, 43–46.
Schelten, J. & Hendricks, R. W. (1978). *J. Appl. Cryst.* **11**, 297–324.
Schwahn, D., Miksovsky, A., Rauch, H., Seidl, E. & Zugarek, G. (1985). *Nucl. Instrum. Methods Phys. Res. A*, **239**, 229–234.
Sears, V. F. (1984). *Thermal-Neutron Scattering lengths and Cross Sections for Condensed-Matter Research*, Atomic Energy of Canada Limited Report AECL-8490.
Shapiro, S. M. & Chesser, N. J. (1972). *Nucl. Instrum. Methods*, **101**, 183–186.
Shull, C. G., Billman, K. W. & Wedgewood, F. A. (1967). *Phys. Rev.* **153**, 1415–1422.
Stehn, J. R., Goldberg, M. D., Magurno, B. A. & Wiener-Chasman, R. (1964). *Neutron Cross Sections*. Brookhaven National Laboratory Report No. BNL 325, 2nd ed.
Takahashi, T. & Hashimoto, M. (1995). *Phys. Lett. A*, **200**, 73–75.
Takahashi, T., Hashimoto, M. & Nakatani, S. (1999). *J. Phys. Chem. Solids*, **60**, 1591–1594.
Treimer, W., Strobl, M. & Hilger, A. (2001). *Phys. Lett A*, **289**, 151–154.
Treimer, W., Strobl, M. & Hilger, A. (2002). *Phys. Lett A*, **305**, 87–92.
Villa, M., Baron, M., Hainbuchner, M., Jericha, E., Leiner, V., Schwahn, D., Seidl, E., Stahn, J. & Rauch, H. (2003). *J. Appl. Cryst.* **36**, 769–773.
Wagh, A. G., Rakhecha, V. C. & Treimer, W. (2001). *Phys. Rev. Lett.* **87**, 125504.
Zachariasen, W. H. (1967). *Theory of X-ray Diffraction in Crystals*, pp. 142. NewYork: Dover.